Chlorine K-Edge X-ray Absorption Spectroscopy as a Probe of Chlorine−Manganese Bonding: Model Systems with Relevance to the Oxygen Evolving Complex in Photosystem II†

Annette Rompel,[1a,b] Joy C. Andrews,[1b,c] Roehl M. Cinco,[1b,d] Michael W. Wemple,[1e] George Christou,[1e] Neil A. Law,[1f] Vincent L. Pecoraro,[1f] Kenneth Sauer,*[,1b,d] Vittal K. Yachandra,*[,1b] and Melvin P. Klein*[,1b]

Contribution from the Structural Biology Division, Lawrence Berkeley National Laboratory, Berkeley, California 94720, Department of Chemistry, University of California, Berkeley, California 94720, Department of Chemistry, Indiana University, Bloomington, Indiana 47405, and Department of Chemistry, University of Michigan, Ann Arbor, Michigan 48109

Received April 3, 1996[⊗]

Abstract: For a series of Mn−Cl coordination complexes the chlorine K-edge X-ray absorption spectra (XAS) have been measured to probe chloride−manganese bonding. Results show that in a series of mononuclear (single Mn) compounds with Cl covalently bound to Mn, the intensity of the pre-edge feature increases in the order $Mn^{II} < Mn^{III} < Mn^{IV}$. For a series of distorted cubane complexes (containing 4 Mn) with bridging and terminal Cl ligands, three pre-edge features are seen. The pre-edge peak at lowest energy increases in intensity as more terminal Cl are included in the compounds. The origin of these features in the edge spectra is described in terms of the symmetry and ligand field splittings expected for the Mn complexes. The Mn model systems studied here have potential application to the oxygen evolving complex (OEC) in Photosystem II (PSII), where direct structural evidence for a halide binding site on the Mn cluster in one or more S-states of the Kok cycle would be informative.

Introduction

This paper describes how Cl K-edge X-ray absorption spectroscopy (XAS) of manganese model compounds can be used to probe Cl−Mn bonding. X-ray absorption edge spectroscopy has been used extensively at the K-edge of transition metal centers such as Mn, Fe, Ni, Cu, and Mo. Recently, it has been demonstrated that the absorption edges of ligands such as S and Cl can be used to study the electronic structure of first transition series metal complexes[2−4] and copper-containing metallo proteins.[5] Earlier studies by DeRose found that the Cl K-edge of Mn−Cl model compounds was dependent on the oxidation state of Mn.[6] The 3p orbitals of S and Cl ligands are directly involved in bonding with transition metal ions. Because the electric dipole-allowed transitions for K-edges are 1s → *n*p, ligand K-edge X-ray absorption spectroscopy provides a direct probe of these ligand−metal bonding interactions. The K-edge absorption spectrum of Cl bound to an open shell metal shows a characteristic pre-edge feature. It has been shown that the pre-edge feature in the Cl K-edge spectrum is due to a forbidden 1s → 3d transition, which becomes partially allowed due to mixing of ligand p-orbitals with metal d-orbitals.[2−5] This pre-edge feature is not present when chlorine is not ligated to an open shell transition metal.

The Mn model systems studied here have potential application to the oxygen evolving complex (OEC) in Photosystem II (PSII). Photosynthetic water oxidation is catalyzed by a tetranuclear Mn cluster, known as the OEC, that is bound to the lumenal side of PS II (for recent reviews see ref 7). Both Cl^- and Ca^{2+} are required in the native complex, and removal or substitution of these ions affects the ability of the OEC to advance through the S-state intermediates.[8] The results of steady-state kinetic experiments have been interpreted to indicate a halide binding site on the Mn cluster.[8,9] Despite a multitude of spectroscopic studies, direct structural evidence for such a site has not yet been reported.

A method that should allow us to determine whether Cl is bound to the Mn cluster is Cl K-edge spectroscopy. Direct ligation of Cl to Mn would be confirmed from Cl K-edge XAS of PS II by the presence of a pre-edge feature. It has recently been shown that it is possible to prepare PS II samples that contain only one functional Cl^-/PS II.[9c] Therefore, it is possible to probe the Cl ligation without interference from adventitious Cl in the PS II samples. This study investigates the Cl K-edge spectra of Mn−Cl compounds and forms the foundation for future Cl K-edge XAS studies of the OEC in PS II.

† Abbreviations: FWHM: full width at half maximum; HOMO: highest occupied molecular orbital; OEC: oxygen evolving complex; PS II: Photosystem II; XAS: X-ray absorption spectroscopy.

* To whom correspondence should be addressed.

⊗ Abstract published in *Advance ACS Abstracts,* April 15, 1997.

(1) (a) Present address: Westfälische Wilhelms-Universität Münster. (b) Lawrence Berkeley National Laboratory. (c) Present address: California State University, Hayward. (d) University of California, Berkeley. (e) Indiana University, Bloomington. (f) University of Michigan, Ann Arbor.

(2) (a) Shadle, S. E.; Hedman, B.; Hodgson, K. O.; Solomon, E. I. *J. Am. Chem. Soc.* **1995**, *117*, 2259−2272. (b) Shadle, S. E. Ph.D. Dissertation, Stanford University, Stanford, CA, 1994.

(3) Shadle, S. E.; Hedman, B.; Hodgson, K. O.; Solomon, E. I. *Inorg. Chem.* **1994**, *33*, 4235−4244.

(4) Hedman, B.; Hodgson, K. O.; Solomon, E. I. *J. Am. Chem. Soc.* **1990**, *112*, 1643−1645.

(5) Shadle, S. E.; Penner-Hahn, J. E.; Schugar, H. J.; Hedman, B.; Hodgson, K. O.; Solomon, E. I. *J. Am. Chem. Soc.* **1993**, *115*, 767−776.

(6) DeRose, V. J. Ph. D. Dissertation, University of California, Berkeley. Lawrence Berkeley Laboratory Report #LBL-30077, 1990; pp 186−193.

(7) (a) Debus, R. J. *Biochim. Biophys. Acta* **1992**, *1102*, 269−352. (b) Sauer, K.; Yachandra, V. K.; Britt, R. D.; Klein, M. P. In *Manganese Redox Enzymes*; Pecoraro, V. L., Ed.; VCH: New York, 1992; pp 141−176.

(8) Boussac, A.; Rutherford, A. W. *Biochem. Soc. Trans.* **1994**, *22*, 352−358.

(9) (a) Sandusky, P. O.; Yocum, C. F. *Biochim. Biophys. Acta* **1986**, *849*, 85−93. (b) Yocum, C. F. *Biochim. Biophys. Acta* **1991**, *1059*, 1−15. (c) Lindberg, K.; Andréasson, L.-E. *Biochemistry* **1996**, *35*, 14259−14267.

S0002-7863(96)01095-5 CCC: $14.00

Experimental Section

Synthesis and properties of $Mn^{II}(2\text{-MeIm})_3Cl_2$,[10] [2-MeIm = 2-methyl imidazole], $Mn^{III}(salen)Cl$,[11] [H_2salen = *N*,*N*′-disalicylidene-1,2-diaminoethane], $Mn^{IV}(salpn)Cl_2$,[12] [H_2salpn = *N*,*N*′-disalicylidene-1,3-diaminopropane], $Mn^{III}(5\text{-Cl-salpn})(CH_3OH)_2(O_3SCF_3)$[13], $Mn_4O_3Cl(O_2CMe)_3(dbm)_3$[15,16] [dbm = dibenzoylmethane], $Mn_4O_3Cl_4(O_2CMe)_3(py)_3$ [py = pyridine][17] and $[Hpy]_3Mn_4O_3Cl_7(O_2CMe)_3$[16] have been previously described. $MnCl_2{\cdot}4H_2O$ was of reagent grade, purchased from Baker, and used as received.

Collection of Cl K-edge Spectra. Cl K-edge spectra were recorded at the Stanford Synchrotron Radiation Laboratory (SSRL) using the 54-pole wiggler beamline 6-2, with a Pt-coated focusing mirror and a Si(111) double crystal monochromator. Details of the setup have been described earlier [see refs 2−5 and references therein]. All Cl K-edge spectra were collected at room temperature. The data were collected as fluorescence excitation spectra with a Lytle detector. A small amount of model compound (on the order of μg) was ground into a fine powder and dispersed thinly over about 1 cm^2 on Mylar tape. The compounds were run at successively lower amounts until a constant spectrum was obtained, to avoid loss of resolution due to self-absorption of the sample. Scans were run from 2710 to 3100 eV, with a step size of 0.08 eV from 2810 to 2850 eV to obtain high resolution in the pre-edge and edge region. For energy calibration the Cl K-edge spectra of Cs_2CuCl_4 were run at intervals between the samples. The pre-edge position of Cs_2CuCl_4 was assigned to 2820.20 eV, based on the published value.[3] Reproducibility of the Cl K-edge energies in the above conditions has been previously found[3] to be ±0.1 eV.

A pre-edge background was removed from all spectra by fitting a straight line to the pre-edge region and subtracting this straight line from the entire spectrum. Normalization of the spectra was accomplished by fitting a quadratic function to the data in the far post-edge region and extrapolating to the energy of the first absorption maximum, where the absorbance was set to unity. The pre-edge positions for each Cl K-edge spectrum were initially determined from the energy of the zero crossing of the first derivative. These values were then refined by deconvolution of the spectra as described below. The first inflection-point energy of the steeply rising absorption edge was determined from the zero-crossing of the second derivative of the spectrum. Analytical differentiation of a third-order polynomial fit to the data over an interval of 1.5 eV on each side of a data point produced the derivative spectra.

Fitting of Pre-Edge Peaks. The pre-edge peaks were fit with EDG_FIT, written by Dr. Graham George of SSRL. The peaks are fit to pseudo-Voigt functions, which are a combination of Gaussian and Lorentzian shapes. The pre-edge peaks were best fit with a mix of 50% Gaussian and Lorentzian peaks with a line width ratio of 1:1. For peaks under the edge, a 100% Gaussian lineshape was used. The number of peaks to fit in the pre-edge and edge regions was determined by the number of features in the second derivative. In addition, an arctangent function was fit in the edge region to account for the increase in continuum absorption. Fits were done using three energy ranges: 2818−2826, 2818−2828, and 2818−2830 eV. This was done because the fits differ slightly depending on the energy range chosen for the fit. Second derivatives of the fits were compared with second derivatives of the original data, and only fits whose shape and minima in the second derivative corresponded closely with the original data were accepted. Values for amplitude, energy, and half-width were averaged for each compound from the acceptable fits (4 to 8 fits) using the different energy ranges. Peak areas (intensities) were approximated by the product of peak amplitude times the full width at half height.

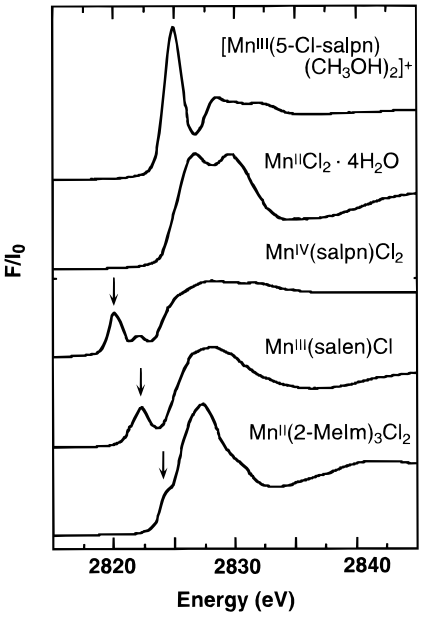

Figure 1. Normalized Cl K-edge X-ray absorption spectra of $Mn^{II}(2\text{-MeIm})_3Cl_2$, $Mn^{III}(salen)Cl$, $Mn^{IV}(salpn)Cl_2$, $Mn^{II}Cl_2{\cdot}4H_2O$, and $[Mn^{III}(5\text{-Cl-salpn})\ (CH_3OH)_2]^+$. Arrows indicate pre-edge features, whose energies are listed in Table 1.

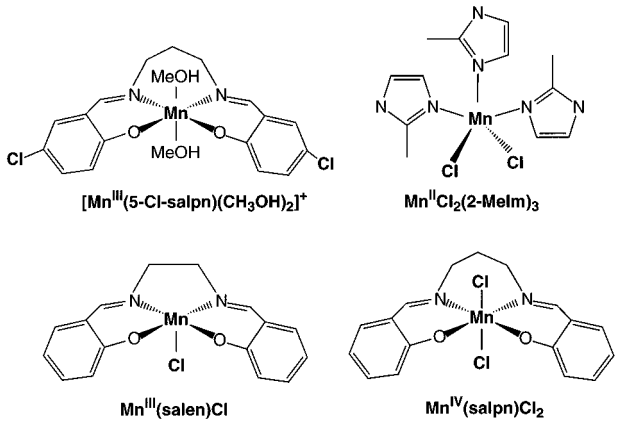

Figure 2. Core structures of Mn−Cl mononuclear model compounds, $Mn^{II}(2\text{-MeIm})_3Cl_2$, $Mn^{III}(salen)Cl$, $Mn^{IV}(salpn)Cl_2$, and $[Mn^{III}(5\text{-Cl-salpn})\ (CH_3OH)_2]^+$.

Results

Mn−Cl Mononuclear Compounds. The Cl K-edge X-ray absorption spectra of $Mn^{II}(2\text{-MeIm})_3Cl_2$,[10] $Mn^{III}(salen)Cl$,[11] $Mn^{IV}(salpn)Cl_2$,[12] $Mn^{II}Cl_2{\cdot}4H_2O$, and $[Mn^{III}(5\text{-Cl-salpn})(CH_3OH)_2][O_3SCF_3]$[13] are presented in Figure 1. The core structures of the Mn−Cl mononuclear complexes are shown in Figure 2. Information on the bond lengths, pre-edge energies, and edge inflection energies as determined from the spectra of these compounds is given in Table 1.

In $Mn^{II}(2\text{-MeIm})_3Cl_2$, $Mn^{III}(salen)Cl$, and $Mn^{IV}(salpn)Cl_2$ chloride is ligated to manganese, and for all three compounds pre-edge features are present. If chloride is part of an organic ring system, as in $[Mn^{III}(5\text{-Cl-salpn})(CH_3OH)_2]^+$, and not a direct ligand of Mn or not covalently bound, as in $Mn^{II}Cl_2{\cdot}4H_2O$, no pre-edge feature is seen. The pre-edge features and the

(10) Phillips, F. L.; Shreeve, F. M.; Skapski, A. C. *Acta Crystallogr.* **1976**, *B32*, 687−692.
(11) Pecoraro, V. L.; Butler, W. M. *Acta Crystallogr.* **1986**, *C42*, 1151−1154.
(12) Law, N. A.; Machonkin, T. E.; McGorman, J. P.; Larson, E. J.; Kampf, J. W.; Pecoraro, V. L. *J. Chem. Soc., Chem. Commun.* **1995**, 2015−2016.
(13) Larson, E. J.; Pecoraro, V. L. *J. Am. Chem. Soc.* **1991**, *113*, 3810−3818.
(14) Smith, T. A.; DeWitt, J. G.; Hedman, B.; Hodgson, K. O. *J. Am. Chem. Soc.* **1994**, *116*, 3836−3847.
(15) Wang, S.; Folting, K.; Streib, W. E.; Schmitt, E. A.; McCusker, J. K.; Hendrickson, D. N.; Christou, G. *Angew. Chem., Int. Ed. Engl.* **1991**, *30*, 305−306.
(16) Wang, S.; Tsai, H.-L.; Libby, E.; Folting, K.; Streib, W. E.; Hendrickson, D. N.; Christou, G. *Inorg. Chem.* **1996**, *35*, 7578−7589.
(17) Hendrickson, D, N.; Christou, G.; Schmitt, E. A.; Libby, E.; Bashkin, J. S.; Wang, S.; Tsai, H.-L.; Vincent, J. B.; Boyd, P. D. W.; Huffman, J. C.; Folting, K.; Li, Q.; Streib, W. E. *J. Am. Chem. Soc.* **1992**, *114*, 2455−2471.

Table 1. Bond Length for Terminal and Bridging Cl Ligands of Mn Coordination Compounds and Cl K-Edge Pre-Edge Energies and Rising Edge Inflection Points

compd	bond length: terminal Cl [Å]	bond length: bridging Cl [Å]	pre-edge energy[a] [eV]	edge inflection[b] [eV]	ref
$Mn^{II}(2\text{-MeIm})_3Cl_2$	2.525, 2.392		2823.8[c]	2825.4	9
$Mn^{III}(salen)Cl$	2.461		2822.3	2825.0	10
$Mn^{IV}(salpn)Cl_2$	2.290, 2.253		2820.1, 2822.1	2823.9	11
$Mn_4O_3Cl(O_2CMe)_3(dbm)_3$		μ_3: 2.641, 2.656, 2.654	2820.6, 2822.0, 2823.3	2825.7	15,16
$Mn_4O_3Cl_4(O_2CMe)_3(py)_3$	2.229[d]	μ_3: 2.629[d]	2820.6, 2821.7, 2823.3	2826.2	17
$[Hpy]_3Mn_4O_3Cl_7(O_2CMe)_3$	2.27[d]	μ_3: 2.65[d]	2820.5, 2821.9, 2823.2	2825.7	16

[a] The precision of these energies, as determined by using different polynomial fits to the data over an interval is $<\pm 0.05$ eV. [b] The precision of the inflection point energy is $<\pm 0.1$ eV; the inflection point reported is determined from the zero-crossing of the second derivative of the spectrum. [c] The zero-crossing of the first derivative in the pre-edge region was taken as the pre-edge energy. [d] C_3 symmetry.

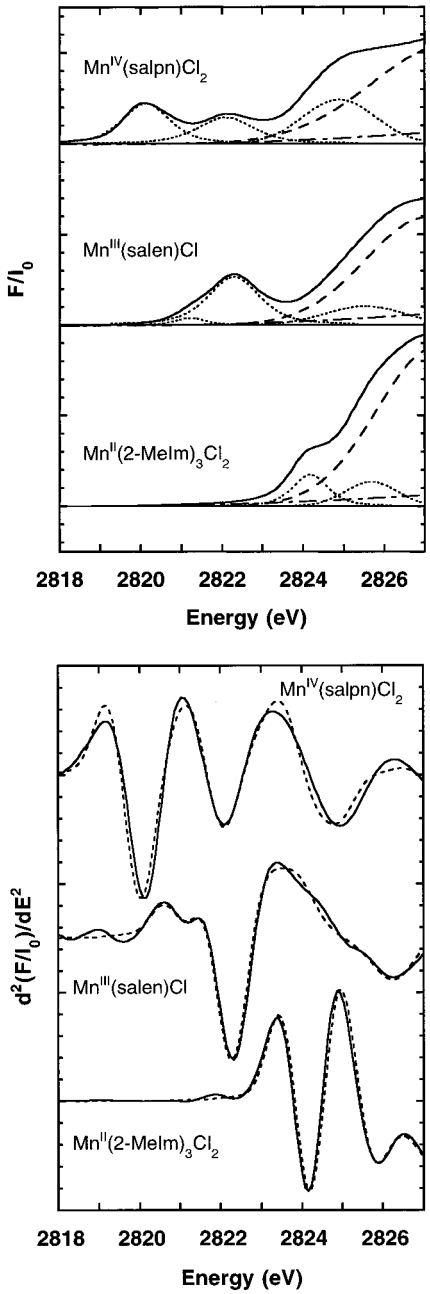

Figure 3. (A) Pre-edge peak region of the normalized Cl K-edge spectra of $Mn^{II}(2\text{-MeIm})_3Cl_2$ (bottom), $Mn^{III}(salen)Cl$ (middle), and $Mn^{IV}(salpn)Cl_2$ (top). Components of fits (dotted lines ···) made using EDG_FIT are shown under the data (solid lines —). The tail of the arctangent function is shown with a dash dot line (— · —). The peak under the edge is shown with a dashed line (- -). (B) Second derivatives of the pre-edge peak region of the original data of the above three compounds (solid line —) and second derivatives of fits to the data (dashed line - -).

second derivatives for the compounds with pre-edge features are shown in Figure 3.

The edge energy is at 2825.4 eV for $Mn^{II}(2\text{-MeIm})_3Cl_2$. In $Mn^{III}(salen)Cl$ and in $Mn^{IV}(salpn)Cl_2$ the edge shifts to lower energy (2825.0 and 2823.9 eV, respectively). Shadle et al.[2] showed that the main absorption results from a Cl 1s → 4p transition. The edge inflection energy directly reflects the Cl 1s core energy level and can be related to the relative charge donated by the ligand in the complex. The edge position for noncovalently bound Cl as in $Mn^{II}Cl_2 \cdot 4H_2O$ occurs at 2825.4 eV.

In $[Mn^{III}(5\text{-Cl-salpn})(CH_3OH)_2]^+$ Cl is bound to the 5-position on the phenyl ring. The edge position is at 2824.2 eV. The observed spectral features found for $[Mn^{III}(5\text{-Cl-salpn})(CH_3OH)_2]^+$ are very similar to the ones found for 9,10-dichloroanthracene.[14] Single crystal measurements[14] revealed that the single intense feature is due primarily to a Cl 1s → σ^* transition. The broad higher energy features have been attributed to the C−Cl environment.

Fitting of Pre-Edge Peaks of Mn−Cl Mononuclear Compounds. Deconvolutions that result from fitting of the pre-edge region of the Mn−Cl mononuclear compounds are shown in Figure 3A, along with a comparison of the second derivative of the data and the second derivative of a representative fit (Figure 3B). Values for energy, full width at half maximum (FWHM), and intensities of the pre-edge peaks are given in Table 2. The second derivative and fitting of the pre-edge region of $Mn^{II}(2\text{-MeIm})_3Cl_2$ indicate that there is one pre-edge feature, appearing as a shoulder on the rising edge. The energy of this feature was first determined from the zero crossing of the first derivative of the original data to be 2823.8 eV, but it is better resolved by spectral deconvolution to be 2824.2 eV. The intensity of this pre-edge peak is 0.166 ± 0.027, based on the area measurements and normalized spectra as described in the Experimental Section.

The $Mn^{III}(salen)Cl$ compound has two peaks in the pre-edge region, as revealed by the second derivative. The first, at a fit energy of 2821.2 eV, is quite small with a peak area of 0.034 ± 0.008; the second, fit at 2822.3 eV, has a peak area of 0.365 ± 0.052, for a total pre-edge intensity of 0.399 ± 0.055. The peak position of the large pre-edge feature is in agreement with that determined by the zero crossing of the first derivative of the original data (2822.3 eV).

$Mn^{IV}(salpn)Cl_2$ has two pre-edge features, with average areas of 0.300 ± 0.006 and 0.243 ± 0.027, for a total pre-edge intensity of 0.544 ± 0.025. The pre-edge peak positions for this compound as determined by the fits are all essentially the same as those determined from the zero crossings of the first derivative of the data.

Mn−Cl Tetranuclear Compounds. The Cl K-edge spectra of a series of tetranuclear Mn−Cl compounds are shown in Figure 4. The core structures of these compounds, a distorted-

Table 2. Pre-Edge Fits of Cl K-Edges of Mn−Cl Compounds

compd	energy[a]	energy[b]	amplitude	FWHM	area[c]	total area
$Mn^{II}(2\text{-MeIm})_3Cl_2$	2823.8	2824.2	0.337 ± 0.027	0.491 ± 0.045	0.166 ± 0.027	0.166 ± 0.027
Mn^{III}(salen)Cl		2821.2	0.079 ± 0.011	0.425 ± 0.061	0.034 ± 0.008	
	2822.3	2822.3	0.524 ± 0.015	0.696 ± 0.085	0.365 ± 0.052	0.399 ± 0.055
Mn^{IV}(salpn)Cl_2	2820.1	2820.1	0.444 ± 0.003	0.677 ± 0.009	0.300 ± 0.006	
	2822.1	2822.1	0.281 ± 0.014	0.866 ± 0.080	0.243 ± 0.027	0.544 ± 0.025
$Mn_4O_3Cl(O_2CMe)_3(dbm)_3$	2820.6	2820.5	0.238 ± 0.007	0.544 ± 0.040	0.129 ± 0.011	
	2822.0	2821.8	0.238 ± 0.014	0.787 ± 0.015	0.187 ± 0.013	
	2823.3	2823.2	0.344 ± 0.007	0.666 ± 0.044	0.229 ± 0.015	0.546 ± 0.013
$Mn_4O_3Cl_4(O_2CMe)_3(py)_3$	2820.6	2820.5	0.453 ± 0.007	0.567 ± 0.021	0.256 ± 0.012	
	2821.7	2821.7	0.307 ± 0.006	0.769 ± 0.027	0.236 ± 0.011	
	2823.3	2823.3	0.298 ± 0.029	0.837 ± 0.064	0.251 ± 0.042	0.746 ± 0.047
$[Hpy]_3Mn_4O_3Cl_7(O_2CMe)_3$	2820.5	2820.4	0.555 ± 0.008	0.598 ± 0.029	0.332 ± 0.020	
	2821.9	2821.8	0.313 ± 0.015	0.771 ± 0.008	0.241 ± 0.011	
	2823.2	2823.3	0.358 ± 0.025	0.763 ± 0.051	0.226 ± 0.026	0.799 ± 0.048

[a] Energies in eV from zero crossing of first derivative. Repeatability is ±0.1 eV. [b] Energies in eV from spectral deconvolution using EDG_FIT. Standard deviations are for all fits for which the second derivative was acceptable, as described in the Experimental Section, were less than 0.1 eV. [c] Peak area is approximated as amplitude times FWHM.

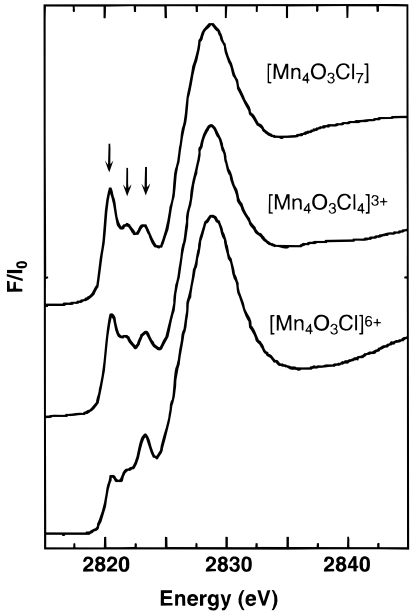

Figure 4. Normalized Cl K-edge X-ray absorption spectra of $Mn_4O_3Cl(O_2CMe)_3(dbm)_3$, $Mn_4O_3Cl_4(O_2CMe)_3(py)_3$, and $[Hpy]_3Mn_4O_3Cl_7(O_2CMe)_3$. Arrows indicate the three pre-edge features.

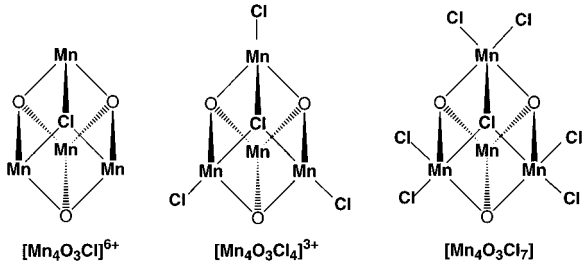

Figure 5. Core structures of Mn−Cl tetranuclear model compounds, $Mn_4O_3Cl(O_2CMe)_3(dbm)_3$, $Mn_4O_3Cl_4(O_2CMe)_3(py)_3$, and $(Hpy)_3[Mn_4O_3Cl_7(O_2CMe)_3]$.

cubane having a μ_3-Cl bridge to three Mn^{III} with additionally a Mn^{IV} atom at the apex, are shown in Figure 5. The edge energies (Table 1) for these three compounds are approximately the same: 2825.7 eV for compound $Mn_4O_3Cl(O_2CMe)_3(dbm)_3$[15] which contains one Cl bridging to three Mn^{III} atoms, 2826.2 eV for $Mn_4O_3Cl_4(O_2CMe)_3(py)_3$[16] which contains a μ_3-bridging Cl and three terminal Cl ligands, and 2825.7 eV for $[Hpy]_3Mn_4O_3Cl_7(O_2CMe)_3$[16] which has six terminal Cl atoms and one μ_3-bridging Cl, much like the structure of $Mn_4O_3Cl_4(O_2CMe)_3(py)_3$ but with two terminal Cl bound to each Mn^{III} atom. The Mn_4O_3Cl compound has three pre-edge features, which are fit as described below. In the Cl K-edge spectrum of the $Mn_4O_3Cl_4$ compound there are three pre-edge peaks, as in the spectrum of Mn_4O_3Cl, but there is an increase in the amplitude of the lowest-energy pre-edge peak relative to those of the second and third pre-edge peaks, probably due to the addition of terminal Cl−Mn interactions. The $Mn_4O_3Cl_7$ compound also has three pre-edge peaks; and the first is further increased in amplitude relative to those of $Mn_4O_3Cl_4$ and Mn_4O_3Cl, probably due to the contribution of additional terminal Cl ligands. Differences in the peak intensities are presented below.

Fitting of Pre-Edge Peaks of Mn−Cl Tetranuclear Compounds. Components of the fits of pre-edge peaks of Mn−Cl tetranuclear compounds are shown in Figure 6A. It is interesting to note that three pre-edge peaks are seen in all of the complexes, including Mn_4O_3Cl which contains bridging Cl only. The peak energies, widths, and intensities for these compounds are given in Table 2.

The peak energies for the three pre-edge peaks remain essentially the same for all three compounds, differing less than the ±0.1 eV repeatability for the spectra, and the widths of the two lower energy peaks do not differ much, either. The intensity of the lowest-energy peak increases from 0.129 ± 0.011 in Mn_4O_3Cl to 0.256 ± 0.012 in $Mn_4O_3Cl_4$ to 0.332 ± 0.020 in $Mn_4O_3Cl_7$. The intensity of the second pre-edge peak at ∼2820 eV increases as terminal chlorines are added, from 0.187 ± 0.013 to 0.236 ± 0.011 to 0.241 ± 0.011, respectively. The intensities of this second peak for the compounds containing terminal Cl are very close to each other, indicating a change in covalency from bridging Cl to terminal, which does not change significantly upon further addition of terminal Cl. The intensity of the highest energy pre-edge peak stays about the same for all three compounds.

Discussion

Cl K-edge studies of Mn−Cl model compounds provide information on the nature of Mn-halide bonding. The presence of pre-edge features, due to forbidden 1s-3d transitions, indicates mixing of metal 3d orbitals with Cl 3p orbitals. The pre-edge features are transitions from the Cl 1s core orbital to the unoccupied or partially occupied molecular orbitals with Cl 3p and Mn 3d character. The intensity of the pre-edge features gives information on the degree of covalency between the metal and halide,[4] and the pre edge position is affected by the effective charge on the Cl and the energy of the metal orbitals involved

in bonding.[5] We will examine the contribution of the molecular symmetry and ligand field splittings of the d-orbitals to the pre-edge energies and intensities.

Mn−Cl Mononuclear Compounds. The $Mn^{II}(2Me\text{-}Im)_3Cl_2$ complex has distorted trigonal bipyramidal geometry.[10] For a regular trigonal bipyramidal geometry one would expect orbital d_{xz} and d_{yz} at the lowest energy, d_{xy} and $d_{x^2-y^2}$ at the next highest energy, and the d_{z^2} at the highest energy. However, only one pre-edge peak is seen for this compound, as a shoulder on the rising edge. There is an additional small peak under the edge (Figure 3A, bottom). The fits do not converge without this peak, and its presence is indicated by the second derivative as well. This may be indicative that there are additional transitions under the edge that are not easily resolved. The ligand field splittings for Mn^{II} are expected to be smaller than for Mn^{III} or Mn^{IV} and hence may not be resolved in this experiment.

No definitive d−d transitions have been observed by UV−vis spectroscopy for the Mn^{III} monomers, because for this and the Mn−Cl salpn complexes, the UV−vis spectra tend to be dominated by charge-transfer bands.[11,12] Nevertheless, for the five-coordinate square pyramidal Mn^{III} complex with its pseudo-Jahn−Teller axis along the long (2.461 Å) Cl−Mn bond, we predict an order, from lowest to highest energy, of d_{xz} and d_{yz} followed by d_{xy}, d_{z^2}, and $d_{x^2-y^2}$ orbitals. One large pre-edge peak is seen for this complex, with a small shoulder at lower energy. The small shoulder could be due to transitions to the lowest energy Cl 3p- Mn d_{xz} and d_{yz} orbitals and the larger peak at higher energy could be due to transitions to orbitals with metal d_{z^2} character. As in the case with the Mn^{II} compound, there is an additional peak under the edge, as indicated by the fits and the second derivative, which may be due to transitions to molecular orbitals with both Cl 3p and metal 4s character. These are bound states that are higher in energy than the HOMO but lower in energy than the Cl 4p energy level. The intense dipole-allowed transitions to the Cl 4p level give rise to the main edge jump.[2b]

For $Mn^{IV}(salpn)Cl_2$, the overall complex is roughly octahedral but might better be described as D_{4h} because the weaker Cl donors are in the axial positions. The stronger (and qualitatively similar) equatorial N and O donor atoms of the salpn ligand give the Mn atom an approximately axial environment. X-ray crystallography demonstrates this: Mn−Cl bond lengths are 2.29 and 2.25 Å, Mn−O bond lengths are 1.87 and 1.86 Å, and Mn−N bond lengths are 2.02 and 2.03 Å. The EPR spectra also indicate that the electronic environment is axial.[12] If we approximate the environment around the Mn as D_{4h} with an "elongated axis", then the d-orbital energies for the Mn^{IV} compound would be, from lowest to highest, d_{xz} and d_{yz} (degenerate), d_{xy}, then d_{z^2}, followed by $d_{x^2-y^2}$.

Two pre-edge peaks are seen for the Mn^{IV} compound, again possibly due to transitions to orbitals with Cl 3p- Mn d_{xz} and d_{yz} character at lower energy, and transitions to orbitals with metal d_{z^2} character at higher energy, within the D_{4h} approximation. As in the case with the above two compounds, there is a possibility that there is another transition to an orbital with metal d character under the edge, as indicated by the fits and the second derivative.

This series of Mn−Cl mononuclear compounds contains Mn in different oxidation states. For the different oxidation states, the energy of the pre-edge features appears in the order $Mn^{II} > Mn^{III} > Mn^{IV}$, as discussed above. Shadle et al.[2,3] have shown that the pre-edge energy is related to the charge on the ligand and to the metal-derived d-orbital energy. Several factors have an effect on the pre-edge energies and intensities. The charge donation of Cl ligands depends on the coordination geometry. For example, bridging Cl atoms donate more total charge than terminal chlorides; thus, there is a larger covalent contribution to the HOMO (highest occupied molecular orbital) for bridging chlorides. An increase in the coordination number or an increase in charge donation by the ligands (resulting in a less positively charged metal ion) has been shown to result in an increase in the overall energy of the d-manifold of the metal. Furthermore the Cl−Mn bonding is dependent on the nature of the other coordinating ligands. However, the trend observed here can be explained by the fact that the energy of the 3d manifold of the metal shifts to lower energy with increase in oxidation state, thereby shifting the pre-edge transition to lower energy as well.

The total pre-edge intensity increases in the order $Mn^{II} < Mn^{III} < Mn^{IV}$, from 0.166 ± 0.027 for Mn^{II} to 0.399 ± 0.055 for Mn^{III}, to 0.544 ± 0.025 for Mn^{IV}. In earlier studies of Cl K-edges of compounds with Cl ligated to iron,[2] it was found that the observed pre-edge intensity increased by a factor of three from Fe^{II} to Fe^{III}. The increase in intensity is due in the case of both Mn and Fe to the increase in oxidation state of the metal, which allows greater covalency in the Cl−metal bond due to greater donation of charge by Cl to the metal. However, the symmetry is different in the case of the Fe and Mn compounds, and a direct quantitative comparison is not possible.

It is interesting that the main component of the pre-edge peak for the Mn^{III} compound is at 2822.3 eV, whereas the pre-edge energy for the terminal Cl in the distorted-cubane structures is at 2820.6 eV. The charge on Mn and Cl are different in these two cases. In both cases the Cl ligands are bound to Mn^{III}, but the effective oxidation state of Mn is lower in the distorted-cubane because of charge donation from the bridging Cl. Therefore the energy of the d-manifold is increased in the distorted-cubane complexes. However, in addition, the core 1s energy of terminal Cl is different. The terminal Cl in the distorted cubane complexes are bound to Mn atoms that already have charge donation from the bridging Cl. Therefore the terminal Cl in the distorted cubanes have greater negative charge; presumably this is the predominant effect causing the transition to be at a lower energy.

Mn−Cl Distorted-Cubane Complexes. In the three distorted cubane complexes (see Figure 5 for their core structures) the Mn^{IV} ion is in an essentially octahedral MnO_6 environment with relatively small deviations to C_{3v}, but the more important Mn^{III} ions, to which the Cl atoms are ligated, are severely distorted by a Jahn−Teller elongation. The bridging Cl (and the *trans* acetate oxygen) are on the elongation axis. Defining this axis as the Mn^{III} *z* axis, the two terminal Cl on each Mn^{III} are on the *x* and *y* axes. The Jahn−Teller elongation will cause the d_{z^2} orbital to lie below the $d_{x^2-y^2}$ in energy, and the d-electron configuration at each Mn^{III} will thus be $d_{xz}^1 d_{yz}^1 d_{xy}^1 d_{z^2}^1$. The $d_{x^2-y^2}$ orbital directed toward the terminal Cl will be empty, but the d_{z^2} directed toward the bridging Cl will be singly occupied.

The three pre-edge peaks seen for the Mn_4O_3Cl complex can be assigned to transitions to the metal d_{xy}, d_{xz}, and d_{yz} orbitals (nearly degenerate at the lowest energy), and the next two peaks to transitions to the d_{z^2} at the middle energy and $d_{x^2-y^2}$ at the highest energy, respectively. All three pre-edge peak positions and the half-width for the first two pre-edge peaks, as seen in Table 2, do not change significantly from one compound to the other. This indicates that the energy splitting stays the same for the complexes with bridging Cl only and with bridging and either three terminal or six terminal Cl. It is possible that there is a fourth pre-edge peak due to the transitions from the terminal Cl at about the same energy as the lowest-energy peak for Mn_4O_3Cl, but it is not possible to resolve it in this case. The

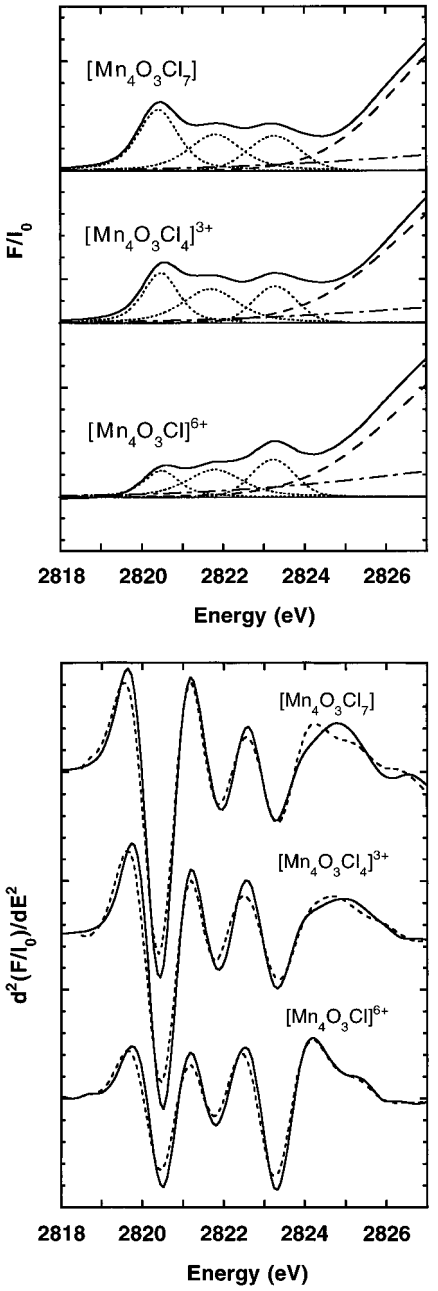

Figure 6. (A) Pre-edge peak region of the normalized Cl K-edge spectra of $Mn_4O_3Cl(O_2CMe)_3(dbm)_3$ (bottom), $Mn_4O_3Cl_4(O_2CMe)_3(py)_3$ (middle), and $[Hpy]_3Mn_4O_3Cl_7(O_2CMe)_3$ (top). Components of fits (dotted lines ···) made using EDG_FIT are shown under the data (solid lines —). The tail of the arctangent function is shown with a dash dot line (— · —). The peak under the edge is shown with a dashed line (- -). (B) Second derivatives of the pre-edge peak region of the original data of the above three compounds (solid line —) and second derivatives of fits to the data (dashed line - -).

second derivatives of the complexes (Figure 6b) all show only three features, indicating that only three pre-edge peaks are resolved.

The intensity of the lowest-energy pre-edge peak increases in the series of Mn_4O_3Cl to $Mn_4O_3Cl_4$ to $Mn_4O_3Cl_7$. These differences are reproducible and reliable, because care was taken to avoid bulk self-absorption, as described in the Experimental Section. It is expected that the 1s energy level of a terminal Cl will be lower than that of a bridging Cl because the electron density of a terminal Cl is greater. A bridging Cl bound to 3 Mn will donate more electron density to the metal, and the 1s to 3d transition will require more energy than that for a terminal Cl, which donates electrons to only one metal center.

The trend in total pre-edge peak intensity for the distorted-cubane series is 0.546 ± 0.013 for Mn_4O_3Cl, 0.746 ± 0.047 for $Mn_4O_3Cl_4$ and 0.799 ± 0.048 for $Mn_4O_3Cl_7$. The pre-edge peak intensity is affected by the number of allowed transitions, which is the same for all three complexes, and by the covalency of the Cl−metal interactions. Although the number of Cl−Mn interactions increases linearly in this series of three complexes, the covalency is not the same for a terminal Cl as for a bridging Cl. As mentioned above, the covalency is much higher for bridging Cl because there is greater donation of charge to the metal d orbitals. The increase in pre-edge intensity from bridging only to three terminal Cl (a difference of 0.200) is greater than the increase from three terminal to six terminal (a difference of 0.100) probably because the three terminal Cl added to $Mn_4O_3Cl_7$ do not contribute much additional covalency. The intensity of the pre-edge peaks is proportional to the degree of charge donation by the Cl as measured by the covalency of the Mn−Cl bond. As mentioned above, the bridging Cl are directed toward the singly occupied Mn d_{z^2}, and terminal Cl are directed toward the empty $d_{x^2-y^2}$ orbitals. Thus the bridging Cl provides more covalency than the terminal Cl. The intensities are dependent not only on the number of Cl but also on the degree of covalency they bring to the Mn−Cl bonds. This explains why the peaks corresponding to bridging Cl are more intense than those from terminal Cl in the distorted cubane complexes.

Concluding Comments

We have demonstrated the feasibility of Cl K-edge X-ray absorption spectroscopy to probe Cl−Mn bonding. If chloride is covalently bound to Mn, a pre-edge feature is present, whereas, if it is part of an organic ring system or is not covalently bound, no pre-edge feature is seen. This forms the basis for future Cl XAS studies to probe the question of direct ligation of Cl to the Mn cluster of the OEC in one or more S-states of the Kok cycle.

Acknowledgment. We thank Dr. Victoria J. DeRose for her initial work on Cl K-edges of Mn−Cl compounds. We thank Dr. Matthew J. Latimer, Dr. Wenchuan Liang, Gary T. Olsen, John H. Robblee, and Henk Visser for help with XAS data collection. We are grateful to Dr. Britt Hedman of Stanford Synchrotron Radiation Laboratory for help with the experiment. We thank Dr. Michael J. Baldwin for preparation of some of the Mn compounds. We thank the reviewers for their constructive criticism and valuable suggestions. This work was supported by the Director, Division of Energy Biosciences, Office of Basic Energy Sciences, and by the Office of Energy Research, Office of Health and Environmental Research and Health Effects Research, U.S. Department of Energy (DOE) under contract DE-AC03-76SF00098. V.L.P. and G.C. are supported by the National Institute of Health (Grants GM 39406 and GM 39083, respectively). The Stanford Synchrotron Radiation Laboratory is supported by the U.S. Department of Energy. The Biotechnology Laboratory at SSRL is supported by the National Center for Research Resources of the National Institutes of Health. A.R. was supported by a Forschungsstipendium of the Deutsche Forschungsgemeinschaft, which is gratefully acknowledged.

JA9610951